

Ca, Fe, and Mg Trends Among and Within Elliptical Galaxies

Guy Worthey¹, Briana A. Ingermann, and Jedidiah Serven¹

Department of Physics and Astronomy, Washington State University, Pullman, WA 99164-2814, USA

ABSTRACT

In a sample of elliptical galaxies that span a large range of mass, a previously unused Ca index, CaHK, shows that $[\text{Ca}/\text{Fe}]$ and $[\text{Ca}/\text{Mg}]$ systematically decrease with increasing elliptical galaxy mass. Metallicity mixtures, age effects, stellar chromospheric emission effects, and low-mass initial mass function (IMF) boost effects are ruled out as causes. A $[\text{Ca}/\text{Fe}]$ range of less than 0.3 dex is sufficient to blanket all observations. Feature gradients within galaxies imply a global Ca deficit rather than a radius-dependent phenomenon. Some, but not all, Type II supernova nucleosynthetic yield calculations indicate a decreasing Ca/Fe yield ratio in more massive supernovae, lending possible support to the hypothesis that more massive elliptical galaxies have an IMF that favors more massive stars. No Type II supernova nucleosynthetic yield calculations show significant leverage in the Ca/Fe ratio as a function of progenitor metallicity. Therefore, it seems unlikely that the Ca behavior can be explained as a built-in metallicity effect, and this argues against explanations that vary only the Type II to Type Ia supernova enrichment ratio.

Subject headings: Galaxies: abundances — Galaxies: elliptical and lenticular, cD — Galaxies: formation — Galaxies: stellar content

1. INTRODUCTION

The determination of age and metallicity spreads of the stars that compose galaxies is highly useful for better understanding the formation and evolution of the content of the universe. Galaxies that show little evidence for present-day star formation, such as elliptical galaxies, are better laboratories for unraveling the stellar populations than star-forming galaxies plagued by dust, nebulae, and bursty recent star formation.

It is now well established that other galaxies, large elliptical galaxies in particular, display chemical abundances differing that of our own Galaxy. Nonsolar abundance ratios in elliptical galaxies were first mentioned as a possibility by O'Connell (1976) and Peterson (1976), both of whom found Na and Mg features to be strong compared to Fe and Ca features. That $[\text{Mg}/\text{Fe}]$ was

truly greater than zero in large elliptical galaxies, and not just a side effect of an overall lockstep enhancement, was solidified by other studies (e.g., Peletier 1989; Worthey et al. 1992; Faber et al. 1992; Davies et al. 1993; Kuntschner 2000; Serven 2010), establishing the implication that there exists an overall enhancement of some lighter elements relative to iron.

Magnesium and other even- Z elements lighter than the iron peak are made via capture of alpha particles, starting with ^{12}C , and going on to include O, Ne, Mg, Si, S, Ar, Ca, and possibly Ti, where Ti might be too close to the Fe peak elements to be included. Workers tend to expect these elements to track one another due to their common nucleosynthetic origin (Wheeler et al. 1989). So Ca abundance should track Mg abundance according to this logic.

Emerging observations of Ca indices, however, indicate that Ca tends not to follow Mg very well. Up to now, there have been four calcium feature indices used to measure calcium abundance in galaxies. These are Ca4227 and Ca4455 (Trager et al. 1998; Worthey 1998), the Ca II

¹Visiting Astronomer, Kitt Peak National Observatory, National Optical Astronomy Observatory, which is operated by the Association of Universities for Research in Astronomy (AURA) under cooperative agreement with the National Science Foundation.

“triplet” at $\approx 8500\text{\AA}$ (Cenarro et al. 2003), and Ca4227_r (Prochaska et al. 2005).

The Ca4227 , Ca4455 , and Ca II triplet indices suggest a mild decrease or a nearly flat level of $[\text{Ca}/\text{Fe}]$ with increasing $[\text{Mg}/\text{Fe}]$ (Vazdekis et al. 1997; Worthey 1998; Trager et al. 1998; Henry & Worthey 1999; Saglia et al. 2002; Thomas et al. 2003; Cenarro et al. 2003, 2004; Smith et al. 2009). Interestingly and uniquely, the Ca4227_r index produces results to the contrary; higher obtained $[\text{Ca}/\text{Fe}]$ abundances follow more closely the trend of $[\text{Mg}/\text{Fe}]$ (Prochaska et al. 2005). That index was designed to cut out some CN absorption at the expense of requiring accurate relative spectrophotometry.

In terms of observed indices versus galaxy velocity dispersion, Mg-sensitive indices exhibit strong correlations with galaxy velocity dispersion (thus, roughly, galaxy mass), while a much more modest correlation exists for Fe-peak indices (Worthey 1998). The Ca II triplet shows a modest anticorrelation between Ca and central velocity dispersion (Saglia et al. 2002; Cenarro et al. 2003, 2004), while the trend with Ca4227 and Ca4455 is nearly flat (Trager et al. 1998; Cenarro et al. 2004; Smith et al. 2009). Sample size and velocity dispersion range from 28 to 147 galaxies and $\sigma = 40\text{--}370\text{ km s}^{-1}$, respectively, with no obvious trend in results dependent on either of these sample parameters (Saglia et al. 2002; Thomas et al. 2003; Cenarro et al. 2003, 2004; Smith et al. 2009). The trend of Ca4227_r is increasing with increasing velocity dispersion (Prochaska et al. 2005), however, the authors limited their sample of 175 early-type galaxies to those with a velocity dispersion of $\sigma \leq 230\text{ km s}^{-1}$ out of the full range of $\sigma = 50\text{--}300\text{ km s}^{-1}$.

An explanation discussed by Saglia et al. (2002) and Cenarro et al. (2003, 2004) involves the steepening of the initial mass function (IMF) at the low-mass end to make more dwarfs. This would increase Na strength (Spinrad & Taylor 1971) and decrease CaT strength, both of which phenomena are observed in high-mass elliptical galaxies. While it seems appealing to solve two observational effects with one astrophysical reason, boosting the number of low-mass stars also greatly increases the near-IR flux, reddening colors involving near-IR passbands, and lowers near-IR M/L ratios, and drastic lower-IMF changes are usu-

ally looked upon with ill favor on those grounds (Saglia et al. 2002; Thomas et al. 2003).

A more mainstream explanation rests on the astrophysics of supernovae. Generally, Type Ia supernovae produce mainly Fe-peak elements, while Type II supernovae produce the lighter metals, and alpha capture elements in particular. Whatever the causes [many are listed in Worthey (1998) and Trager et al. (1998) and include time delays, wind scenarios, IMF changes at the high-mass end, and binarism trends], the Fe-peak could plausibly decouple from the light elements in terms of abundance, but the light elements should be in lockstep with each other. Thus, the separation of the behavior of Mg and Ca is inherently puzzling.

Worthey (1998) proposed that the simplest explanation for the Ca flatness might be due to metallicity-dependent supernova yields, where the production or ejection of Ca is decreased in metal-rich supernovae. This is weakly supported by the studies of Woosley & Weaver (1995), in that $[\alpha/\text{Ca}]$ increases slightly with increasing metallicity, but more recent calculations from Nomoto et al. (2006) show no evidence of this trend, with Ca tracking Mg in supernova yields of all metallicities. The latter study includes metallicities greater than solar. With Occam’s razor thus tentatively defeated, some other effect must be operating to create a trend along the mass sequence of elliptical galaxies, such that low-mass ellipticals, lenticulars, and spirals have a nearly-solar mixture, while very large ellipticals (that sit alone at the high-mass end of all galaxy morphological types) have a light-element enhanced mixture.

Both the observational material and the models used vary quite widely among the workers that have addressed the Ca topic. Since the conclusions also vary, this motivates the measurement of $[\text{Ca}/\text{Fe}]$ in a better way, if possible. In this paper, we approach the calcium puzzle with the Ca II Fraunhofer H and K features that are strong features in cool stars. Elliptical galaxies are largely composed of low-mass, cooler stars, and thus the integrated-light spectra of these galaxies also display these strong features, leading to a nearly ideal index for measuring calcium abundance trends if the stellar features are indeed sensitive to Ca abundance. Although Ca H and K are subject to absorption by the interstellar medium, ellipti-

cal galaxies contain very little interstellar matter. The blue wavelength of the feature ensures that ordinary G and K type stars, mostly main sequence and warmer giants, contribute most of the light, in contrast to the CaT 8600 feature, which is dominated by red giant branch (RGB) tip and asymptotic giant branch (AGB) star light whose numbers, temperatures, and spectra are all less well understood (Buzzoni 1989; Worthey 1994).

In this paper we focus on a particular CaH+K index, defined in Serven et al. (2005) and named CaHK, and discover for the first time an emphatic anticorrelation between CaHK and Mg *b* index strength. We follow in §3 with an exploration of the influence of calcium emission lines on CaHK index strengths and rule out Ca II emission reversals as a possible culprit for calcium underabundance trends. Admixtures of metal poor subpopulations or young subpopulations or dwarf-enriched populations are also ruled out, leaving abundance ratio changes as the only viable explanation. In §4, we add galaxy-internal gradient information and discuss the inferred abundance ratio trends between galaxies and within galaxies. Finally, §5 summarizes the findings and discusses them within the context of basic chemical evolution.

2. MODELS AND DATA

A grid of synthetic stellar spectra resampled to 0.5Å wavelength intervals in the range 3000Å to 10000Å was incorporated into the Worthey (1994) infrastructure (in which evolution choices and spectral library choices are modular; cf. Dotter et al. 2007; Lee et al. 2009; Serven et al. 2010) in order to produce integrated-light models. This spectral grid was repeatedly calculated with small abundance changes, for example, a 0.3-dex increase in calcium abundance, relative to the scaled-solar mixture, so that spectral shape changes due to elemental abundance drifts could be calibrated. A list of 23 elements was included, and the Grevesse & Sauval (1998) abundance list was used as the solar mixture.

A pertinent example of this is given in Fig. 1, which shows the Ca-enhanced spectrum divided by the unenhanced spectrum. Several Ca-sensitive features become obvious. Ca does not form molecules in stars, so the features are due to Ca I or Ca II atomic species. It is obvious

from Fig. 1 that the Ca H and K features give the strongest percentage response to increased Ca abundance. Furthermore, the response is spread over a quite broad wavelength regime compared to the other Ca-sensitive regions of the spectrum, making measurements even easier. Serven et al. (2005) noted that CaHK is a factor of three more sensitive than the CaT indices despite (in their formalism) being at much lower signal to noise ratio (S/N). For the same S/N, CaHK is almost an order of magnitude better.

In order to make an integrated light model population spectrum, new stellar index fitting functions were generated (first cited in Poole et al. 2010). The three sources of stellar spectral data were (1) a variant of the Worthey et al. (1994) Lick spectra with a wavelength scale refined via cross-correlation, (2) the MILES spectral library of Sánchez-Blázquez, P. et al. (2006b), and (3) the Indo-US library of Valdes et al. (2004). The Indo-US library, smoothed to mimic a Gaussian velocity dispersion with $\sigma = 200 \text{ km s}^{-1}$, was adopted as the fiducial set, with the other two adjusted to fit via linear transformations. Both sets, in general, needed more than merely zero-point shifts. In the Lick case, a slope term was sometimes used to account for the difference in spectra resolution. In the MILES case, a slope term was often applied to account for what is probably a scattered light effect, which is discussed in greater depth in Sánchez-Blázquez, P. et al. (2006b).

The data were then fit with multivariate polynomials in five generously overlapping temperature swaths, then summarized in a lookup table that gives each index strength as a function of stellar atmosphere parameters. As described so far, the fits mimic only the run of Galactic star index strengths with a single abundance parameter, $[\text{Fe}/\text{H}]$. In order to add the sensitivity to individual elements, the synthetic spectra were again employed to generate index responses $\partial I / \partial [X/R]$, where X is the element of interest, mostly calcium in this paper, and R stands for “generic heavy element,” and is employed so that the common case of Fe abundance changes can be written as $[\text{Fe}/R]$ and will still make logical sense.

This library of element-sensitive indices was then attached to stellar evolutionary isochrones by choosing a Salpeter (1955) IMF. The isochrone sets used in the modules are modular, but initial

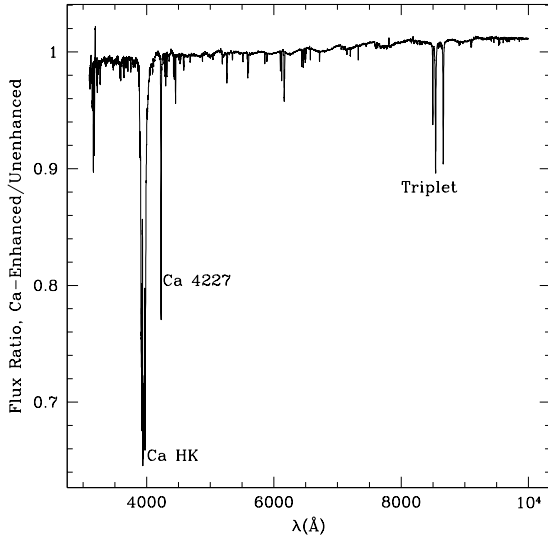


Fig. 1.— Ratio of two model spectra of simple stellar populations of age 15 Gyr and abundance around solar, smoothed somewhat for clarity. The model with calcium raised a factor of two is divided by the unenhanced model. The area of the spectrum that responds best to extra Ca is the Ca HK feature, decreasing 30% over a broad wavelength range. Lesser spectral responses at the red calcium “triplet” and at 4227Å are noted.

testing was done with the Worthey (1994) set. To produce an integrated-light index strength, values of the flux and continuum for each “star” in the isochrone, weighted by number, are added up the isochrone, and then reformed into an index value after summation. Finally, since we compare in the end to spectra that are smoothed to mimic a 300 km s⁻¹, index corrections were calculated using synthetic model spectra smoothed to the relevant velocity dispersions and applied to the model indices.

For observational comparison, we use four data sources for the index measurements. They are the Graves et al. (2007) SDSS averages of non-LINER elliptical galaxies and three sets of high-S/N near-nuclear spectra (Sánchez-Blázquez et al. 2006a; Servén 2010; Servén et al. 2010; Trager et al. 2005, 2008). The Graves average spectra are parceled out into bins of velocity dispersion, covering a wide range. The CaHK index is defined in Servén et al. (2005) and the regular Lick indices are defined in Trager et al. (1998).

The Trager et al. (2008) spectra were kindly provided by the lead author of that paper, already smoothed to 300 km s⁻¹. They are 12 early-type galaxies in the Coma cluster with velocity dispersions between 41 and 270 km s⁻¹, including the cD galaxy NGC 4874, taken with the Low-Resolution Imaging Spectrometer on the Keck II 10 m Telescope. This instrument uses slitlets as spectral apertures, and the reduced spectra were weighted along the slit to mimic a circular aperture of diameter 2.7″. The S/N in a 75 km s⁻¹ bin was between 35 and 292, and one flux standard was observed for purposes of applying a spectral shape correction. We were also kindly provided a subset of 35 of the 98 Sánchez-Blázquez et al. (2006a) long slit spectra, trimmed to a 4″ equivalent (at redshift $z = 0.016$ for a physical size of 0.62 kpc assuming $H_0 = 70$ km s⁻¹ Mpc⁻¹) central aperture. They were obtained at the 4.2m William Herschel Telescope at Roque de los Muchachos Observatory using the ISIS spectrograph and the Cassegrain Twin Spectrograph on the 3.5m German-Spanish Astrophysical Observatory. The 35 elliptical galaxies cover a range of velocity dispersion between 130 and 330 km s⁻¹ and also local density. The spectra are at a range of native instrumental resolution between 3.5Å and 6.6Å (FWHM) and a typical S/N of 50-110 Å⁻¹. A few flux standards were observed

during the runs for purposes of spectra shape correction. We note that CaHK is near the blue edge of the spectral coverage. The Serven (Serven 2010; Serven et al. 2010) spectra of mostly Virgo elliptical galaxies span a range of velocity dispersion from 80 to 360 km s⁻¹ and were obtained with the Cassegrain Spectrograph at the 4 m Mayall telescope at Kitt Peak National Observatory. Nuclear portions of the long slit spectra were extracted at an aperture of 13.8'', corresponding to a physical distance of 1.1 kpc assuming a Virgo cluster distance of 16.47 Mpc (Blakeslee et al. 2009). The S/N is over 100 per 2Å bin except for the dwarf galaxies in the sample. Dozens of flux standard star observations of several flux standards at varying airmasses and with both narrow and wide slits were observed nightly during the KPNO runs for spectra shape correction. Of the various data sets, the Serven (2010) spectra are most likely to have the most reliable spectrophotometric shape, due to the many flux standards observed and also because the CaHK index falls in the middle of the spectral range of the instrument where scattered light was demonstrably negligible, even for red objects, and camera focus issues were never observed.

The apertures sample beyond the half-light radius of each SDSS galaxy but are more nearly nuclear for the high-S/N sets of local galaxies. For galaxies (or average galaxies) with velocity dispersion greater than 300 km s⁻¹, we computed corrections via model spectra the same as for the model indices described above but in the opposite direction. For galaxies with velocity dispersion less than 300 km s⁻¹, extra, wavelength-dependent Gaussian smoothing was applied to bring them to 300 km s⁻¹ before indices were measured.

The CaHK index definition is quite broad to capture most of the absorption signal that is present. This broad wavelength span leads to probable zero-point offsets between data sets due to imperfections in recovering relative spectrophotometric shape, as discussed in Worthey & Ottaviani (1997). There are only two galaxies in common between Serven (2010) and the subset of the Sánchez-Blázquez et al. (2006a) with which we worked, and within the possible offsets between the sets due to aperture effects and small number statistics no mutual zero-point offset in the CaHK index can be unambiguously shown. No other data sets have overlap.

Some basic index behaviors against velocity dispersion are shown in Figure 2. The Mg *b* index correlates strongly with velocity dispersion, with wide range (2Å). Indices $\langle \text{Fe} \rangle = 0.5 \times (\text{Fe}5270 + \text{Fe}5335)$ and Ca4227 correlate at lesser significance. The Ca HK index, in contrast, anticorrelates. The offsets between data sets, highlighted in the bottom panel of Figure 2 by splitting the data into the four separate sets and fitting lines separately, are predominantly due to (relative) spectrophotometric shape effects. The data are fit with the *FITEXY* program from Press et al. (1992) and the resulting two-error least-squares fits are summarized in Table 1.

The behaviors are as observed in the past for the three top indices, all positive correlations, with Mg *b* being the strongest correlation and Ca4227 the weakest. The CaHK slope, however, is negative in all four data sets. The zero point shifts we take in stride for this work since our conclusions are not affected by them, or even by modest slope differences, and we have not tried to aperture-correct the sets. (Such corrections would be stronger for Mg *b* and $\langle \text{Fe} \rangle$ and weaker for CaHK, based on observed gradient strengths.)

With these models and data in hand, we display them together in Figs. 3 and 4, arraying the CaHK index against the $\langle \text{Fe} \rangle$ index in Fig. 3 and against the Mg *b* index in Fig. 4. A second panel is provided in each case, with deltas applied to the data to make the four data sets agree with the average value at a velocity dispersion of 250 km s⁻¹. As in quite a few such index-index plots (Worthey 1998), the galaxies follow a trajectory significantly skewed from Galactic expectations, indicating systematic drifts in abundance ratios away from Galactic trends. In this case, the sense is that the stronger lined elliptical galaxies have a weaker calcium index. Holding age fixed, stronger metallic lines imply higher metallicity. Furthermore, in the case of Mg *b*, Mg *b* correlates with velocity dispersion strongly (Bender et al. 1993), implying that it is the larger galaxies that have the weakest CaHK index. This can be seen via the symbol size coding in Figs. 3 and 4 well; except, perhaps, for the Herschel data set, the small galaxies lie near the models while the large ones are far away.

Iron indices have a weaker correlation with velocity dispersion, indicating that larger ellipticals

TABLE 1
FITS VERSUS VELOCITY DISPERSION

Diagram	Intercept (\AA)	Slope (\AA per km s^{-1})
Mg <i>b</i> , combined	2.55 ± 0.07	0.0070 ± 0.0003
$\langle \text{Fe} \rangle$, combined	1.79 ± 0.04	0.0023 ± 0.0002
Ca4227, combined	0.92 ± 0.04	0.0010 ± 0.0002
CaHK, KPNO	19.99 ± 0.32	-0.0226 ± 0.0018
CaHK, SDSS	22.19 ± 0.43	-0.0091 ± 0.0025
CaHK, Keck	20.83 ± 0.24	-0.0123 ± 0.0012
CaHK, Herschel	25.90 ± 0.12	-0.0241 ± 0.0006

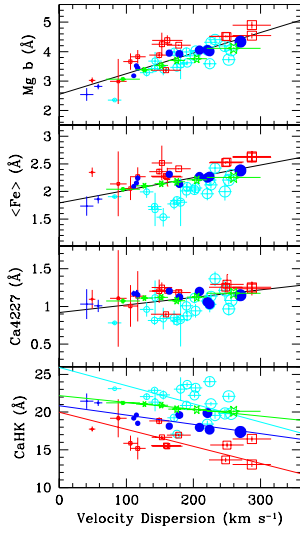


Fig. 2.— Four feature strength indices vs. galaxy central velocity dispersion. Data from Serven (2010); Serven et al. (2010) (red squares), Sánchez-Blázquez et al. (2006a) (light blue open circles), Graves et al. (2007) (green stars), and Trager et al. (2008) (filled blue circles) are plotted with symbol size proportional to velocity dispersion. The lines are two error linear fits to the combined data, except in the bottom panel, where four lines are shown, split by data set to show systematic offsets.

have only slightly more Fe than small ones. That trend is weak, and, indeed, it is still in the realm of possibility that age systematics might be able to drive the Fe trend. Youth drives the stellar population left and down in both of these plots, as seen in the model grid lines.

3. EXPLANATIONS FOR CALCIUM INDEX BEHAVIOR

From the models, it is clear that gross age and metallicity effects cannot account for the diving CaHK index since mixtures of various simple stellar population add approximately like vectors *within* the model grid, but the data points lie outside the grid, even if one were to shift the grid artificially. This leaves four possibilities. One, chromospheric emission (Wilson & Vainu Bappu 1957) may operate with sufficient strength to be an issue. Two, the wavelength difference between CaHK around 3900\AA and the 5100\AA to 5400\AA region where Mg *b* and the Fe indices lie may leave the door open for a small fraction of metal-poor subpopulation to dilute the CaHK index, with the more metal-rich, larger galaxies having less blue flux and hence more fill-in with the weak-lined, blue metal-poor subpopulation. Three, an enriched dwarf population within the galaxy creates a shallower IMF on the low-mass end and weakens the CaHK index as it might for the Ca II triplet feature. Four, the Ca abundance relative to Fe and Mg is changing, diluting with increased galaxy size, with implications for supernova enrichment of the galaxies.

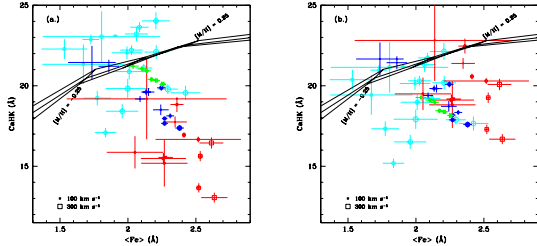


Fig. 3.— CaHK is shown as a function of $\langle v \rangle$. Models based on the Worthey (1994) isochrones are shown, at ages 8, 12, and 17 Gyr, with isometallic lines drawn at scaled solar $[M/H]$ every 0.25 dex. Observational points are drawn with symbol size proportional to galaxy velocity dispersion. Data from Serven (2010); Serven et al. (2010) (red squares), Sánchez-Blázquez et al. (2006a) (light blue open circles), Graves et al. (2007) (green stars), and Trager et al. (2008) (filled blue circles) are plotted. In panel (a) the data are as measured. In panel (b) the CaHK values have been shifted to the average value at 250 km s^{-1} from the index vs. velocity dispersion relations of Table 1.

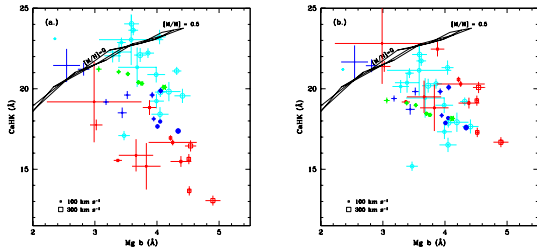


Fig. 4.— CaHK is shown as a function of Mg b. Symbols and lines are as in Fig. 3.

3.1. Chromospheric Emission

Within the centers of the H and K lines, emission spikes are often present for stars of type G0 and later. This was first discovered by Schwarzschild & Eberhard (1913) and was followed up by extensive literature. Wilson & Vainu Bappu (1957) and Wilson (1959) found the logarithms of the widths of these emission lines to be linearly correlated with luminosity, independent of spectral type, although stars of a given luminosity could have a wide range of intensities of the emission. This emission describes general chromospheric activity in stars (Wilson & Vainu Bappu 1957) and is of interest because it results in weaker Ca H and K equivalent width index measurements. We cannot use the previous work directly because we need to judge its effects on the integrated light of stellar populations in the particular index that we are using.

Therefore, we proceeded to estimate the *maximum* amount of emission and its effect on the CaHK index by examining an observational spectra library, choosing that of Valdes et al. (2004) due to spectral resolution and wavelength coverage. For purposes of this exercise, the effective temperatures of the stars were adopted right from the library. Giants of various temperatures, and excluding metal-poor or chemically peculiar stars, were visually examined for emission in the cores of the lines. If emission was spotted, a hand-drawn guess for the true depth of the core was inserted into the spectrum, and the CaHK index measured both with and without the emission spike.

Figure 5 shows the spectra, before and after, of a star with strong emission, HD 200527. After the star is “corrected,” it is smoothed to a galaxy-like velocity dispersion (200 km s^{-1}) that serves as the standard for the index system. Figure 6 shows the results for a collection of K and M giants, specifically $\Delta\text{CaHK} = \text{CaHK}(\text{corrected}) - \text{CaHK}(\text{uncorrected})$. While, as expected, there is quite a lot of scatter in the intensity of the emission, there is also a fairly well-defined maximum edge. We examined many stars hotter than 4500 K, but none of them had any convincing CaII emission. The late-type giants examined here have CaHK index values of order 30 \AA .

In order to complete the test, we approximated the ΔCaHK correction to be a line that is 0.5 \AA at

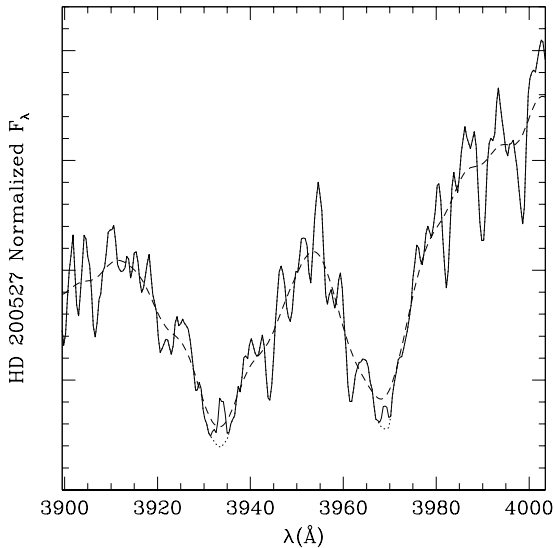


Fig. 5.— Representative set of spectra showing Ca H (λ 3969) and K (λ 3934) features. The plot limits are precisely the index passband of the CaHK index definition, while the pseudocontinua passbands are outside the limits. The solid line is the spectrum from the Indo-US library of Valdes et al. (2004) for M giant HD 200527. The dotted portions of the spectrum show the altered Ca H and K lines to remove emission. The dashed line is the latter spectrum smoothed to mimic a Gaussian velocity dispersion with $\sigma = 200 \text{ km s}^{-1}$.

3000 K and 0.0 \AA at 4500 K and hotter, and then applied this function within the population models of Worthey (1994). At ages 3, 6, and 12 Gyr, the ΔCaHK values were 0.015 \AA , 0.016 \AA , and 0.024 \AA , respectively. The small magnitude of these shifts results from the cool onset of the CaII emission phenomenon, and the rapidly falling continuum levels in these stars, so that these stars have very minimal contribution at the blue wavelengths of Ca H and K. Definitively, then, the hypothesis that CaII emission has anything to do with the peculiar morphology of Figs. 3 and 4 is ruled out.

3.2. Metal-Poor Subpopulations

The second hypothesis, that a varying ratio (in light at 4000 \AA) of metal-poor to metal-rich subpopulations can account for the galaxy trend can also be rejected. Mixtures of populations add approximately like vectors within the model grid. Therefore, one is generally trapped within the confines of the model grid when mixing different populations together, the grids in Figs. 3 and 4 extend between $[\text{Fe}/\text{H}] = -2$ and $[\text{Fe}/\text{H}] = +0.5$ and lie on a roughly linear, roughly orthogonal trajectory. There is no way to produce the galaxy trend with inventive metallicity mixtures, with the caveat that the fairly large wavelength separation between Mg *b* and $\langle\text{Fe}\rangle$ in the green and CaHK in the violet might possibly introduce a nonlinearity.

To investigate this, we concoct some more complex models in Fig. 7. The sequence marked 0%, 5%, and 10% in Fig. 7 is a two-metallicity composite stellar population with the mass fraction of the metal-poor component ($[\text{M}/\text{H}] = -1.5$) as labeled. The age is 8 Gyr for both components, and the metal-rich component starts at $[\text{M}/\text{H}] = 0$ and extends to $[\text{M}/\text{H}] = 0.25$ at the end of the line segment marked with the letter “Z.” The phenomenon of note is the slight twisting of the three line segments as the metal-poor fraction increases. See also Serven et al. (2010), who explore indices that span even further in wavelength.

The twisting is clockwise, and that is in the correct sense to make the model sequences flatten or even decrease with increasing metallicity. The physical reason is that metal-poor populations, dominated by the main sequence stars at this wavelength, are weak-lined: as the metal-rich component drifts yet more metal-rich, its fractional light contribution in the blue decreases

dramatically, giving more weight to the metal-poor component. There are two reasons, however, not to take this very seriously. First, the model would imply that more metal-rich galaxies have a more broad abundance distribution. There is no evidence for this at less than solar $[M/H]$ (Worthey et al. 2005), and, one would think, little motivation to demand such a behavior at higher abundance. Second, metal-poor fractions as high as 10% are probably ruled out by other observations with less than 5% preferred (Worthey et al. 1996) and this leaves the model twists at a very mild level.

Figure 7 also shows the model vectors for bulk age increase and lockstep abundance increase, for basic orientation. It also shows three vectors for Ca, Fe, and Mg abundance mixture tweaks that are useful for the discussion that follows.

3.3. Dwarf Enrichment

The boosted lower IMF hypothesis of Saglia et al. (2002) and Cenarro et al. (2003) can be addressed with the CaHK index as well. Models that include lower main-sequence stars down to $0.1 M_{\odot}$, of age 12 Gyr and of solar composition were computed. These models used Worthey (1994) isochrones due to the availability of low-mass stars in them. The IMF was assumed to be a power law. Slopes of 2.35 (Salpeter 1955) and 5.35 produced CaHK index values of 22.48\AA and 21.04\AA , respectively. However, for this $\Delta\text{CaHK} \sim 1.5\text{\AA}$, the same two IMF slopes gave $V - K$ colors of 3.45 mag and 4.99 mag, respectively. Dust free elliptical galaxies do not have colors much redder than $V - K \approx 3.6$ mag. To get a ΔCaHK from $\sim 0.5\text{\AA}$ up an order of magnitude to the $\sim 5\text{\AA}$ needed to match the observations would require IMF slopes much greater than 5.35. That seems impossible, given the strong infrared color constraint, even if the lower-mass end of the IMF was tapered and fine-tuned to decrease the number of cool dwarfs.

The more modest proposal of van Dokkum & Conroy (2010), who consider slopes of 2.35, 3.0, and 3.5 with the same $0.1 M_{\odot}$ lower cutoff and compare to Wing-Ford and Na I features in the red would probably not violate photometric constraints and would be consistent with our observations. We note that those authors did not consider the hypothesis of enhanced Na abundance, correction for which would drive their results toward more

Salpeter-like slopes.

3.4. Element Ratio Trend

The explanation that remains is that the Ca abundance is changing systematically from smaller elliptical galaxies to larger ones. This is similar to the trends for Mg, Na, and N, (Worthey 1998) although the Ca abundance decreases instead of increases. These trends clearly arise through chemical enrichment processes, and primarily through supernova yields.

The magnitude of the $[\text{Ca}/R]$ abundance spread depends on how conservative one would like to be when interpreting Figs. 3, 4, and 7. If the model-observation separation and $>10\text{\AA}$ CaHK index spreads are to be taken at face value, then the $[\text{Ca}/R]$ variation must be at least -0.15 dex for the weakest-lined galaxies, as illustrated by the vertically-down Ca vector in Fig. 7. Naturally, the trends in $[\text{Fe}/R]$ and $[\text{Mg}/R]$ must also be taken into account, and those elements do affect the CaHK strength, by almost 3\AA for a $[\text{Mg}/R]$ shift of 0.2, sufficient to explain the Mg- σ trend. At face value, that is not sufficient to avoid invoking a $[\text{Ca}/R]$ change. (Note that a positive $\Delta[\text{Fe}/R]$ implies a negative $\Delta[\text{Ca}/\text{Fe}]$.)

If one, not unreasonably, would rather put zero faith in the observational and model zero points, then one is left with relative change vectors, and only the massively-average SDSS data set should be compared with relative model change vectors. This is enabled in Fig. 7, where, looking only at the SDSS data and giving complete zero-point freedom to the models, the vertical change can be explained with the 0.2 Mg enhancement, with the need for an $[\text{Fe}/R]$ boost of about twice what is illustrated; about 0.1 dex in $[\text{Fe}/R]$ (or $[\text{Ca}/\text{Fe}] = -0.1$) while leaving $[\text{Ca}/R]$ unchanged. Or, one could effect the same change with depleted Ca. Either way, and under liberal or conservative assumptions, $[\text{Ca}/\text{Fe}]$ does decrease from small galaxies to large.

As regards calcium, expectations from nucleosynthesis theory are contradictory at the moment. If we look at the work of Nomoto et al. (2006) and Kobayashi et al. (2006) we find that there is a strong metallicity dependence in Na yield that has not been predicted before. This could easily explain the high Na abundance in

massive elliptical galaxies. However, the Ca yields track Ti and Mg very well (normalized by Fe yield), both as a function of supernova progenitor mass and as a function of supernova progenitor initial abundance. However, if we look at the work of Woosley & Weaver (1995) and Timmes et al. (1995) we find a very strong dependence of Ca yield with supernova progenitor mass: Ca decreases relative to Fe, while Ti is about constant and Mg increases with increasing progenitor mass, and the variation is more than the required factor of two. This is in the correct sense to explain our observations if IMF variation (at the high mass end) is the root cause of the abundance trend. In this scenario, a galaxy with higher velocity dispersion will provide star formation environments that are biased toward higher mass star formation. This will chemically enrich the galaxy with the higher mass progenitor yields, and if Woosley & Weaver (1995) yields are used, then it could explain the trend we see.

The other favored explanation for the observed $[\text{Mg}/\text{Fe}]$ trend is a timescale argument in which a longer timescale for enrichment causes Type Ia supernovae to contribute substantially, adding Fe-peak elements to the mixture. However, Type Ia supernovae do not add enough Ca or Ti or lighter elements to generate observable abundance trends within the lighter metals. Therefore, the Ca trend is not readily explainable in this hypothesis, because no published, detailed set of supernova yields has sufficient metallicity dependence (initial metallicity of the progenitor stars, that is) to torque the $[\text{Ca}/\text{Mg}]$ ratios into what we would infer. The Ca evidence therefore tends to disfavor the timescale argument and favor the IMF argument.

4. INTERIOR GRADIENTS

One of our data sets contains spatially resolved indices. In Figs. 8 and 9 we show an additional model grid that has been altered such that Mg is enhanced by a 0.3 dex, and Ca is decreased by 0.3 dex, so that $[\text{Ca}/\text{Fe}] = -0.3$ and $[\text{Ca}/\text{Mg}] = -0.6$ and $[\text{Mg}/\text{Fe}] = +0.3$. The heavy element mass fraction is not (quite) preserved in this altered mixture, and increases a bit because Mg is more abundant than Ca. This modest amount of alteration is sufficient to explain even the most extreme

cases. Therefore we predict that the Ca dilution is less than a factor of two relative to a scaled-solar abundance mixture.

Figs. 8 and 9 also show gradient trends from the Serven (2010) spectra, where the near-nuclear regions are averaged and plotted as crosses, and the more distant regions are averaged and plotted as the endpoints of trend lines. The endpoints are the most distant points available with good data, and the end distance is quite variable, but the main point of the figure is to display the most reliable vector direction. With some exceptions, the gradients tend to lie along the age-metallicity direction indicated by the model grid, and not along a direction more indicative of strong internal gradients in the $[\text{Ca}/\text{Fe}]$ or $[\text{Ca}/\text{Mg}]$ abundances. This is in agreement with previous observations of Mg gradients (Worthey et al. 1992) and indicates a rather global enrichment pattern throughout the galaxy. More recently, Kuntschner et al. (2006) and Rawle et al. (2010) present observational and model-dependent results, respectively, that describe steady, or, on average, perhaps slightly negative Ca abundance gradient trends with increasing galaxy radius. The data presented here are certainly not sufficient to rule out those conclusions.

A straightforward way to homogeneously enrich the volume within a galaxy is to have fairly effective spatial mixing during the enrichment process. Since the process itself is almost certainly supernova blast waves, this seems reasonable. Other mechanisms could also contribute, such as phase mixing of the stars by dynamical effects long after the enrichment phase is over.

5. SUMMARY AND CONCLUSION

Four samples of elliptical galaxies that span a large range of mass are compared to new models that feature a previously unused Ca index, CaHK, and that are also quite flexible in displaying chemical abundance effects on spectra and spectral indices for integrated light. It is seen that $[\text{Ca}/\text{Fe}]$ and $[\text{Ca}/\text{Mg}]$ systematically decrease with increasing elliptical galaxy Mg and Fe line strengths, and, by implication, galaxy mass. Metallicity mixtures and age effects are ruled out as causes due to inability to match the observations. Stellar chromospheric emission was explored but rejected as

being about two orders of magnitude too weak to have any effect on the observed trend. Modulations of the lower IMF increasing the dwarf light fraction do not affect the CaHK index, and thus low-mass IMF variations are also ruled out as a cause.

That leaves chemical abundance variation as the sole remaining explanation. The size of the abundance shifts are modest. Less than a factor of two in Ca dilution can easily explain the trend.

Feature gradients within galaxies imply a tendency toward a pangalactic Ca deficit rather than a strongly radius-dependent phenomenon. The element mixture trend may match a predicted supernova progenitor mass dependence on the Ca yield, although this prediction is not yet firm, apparently. If the mass-dependent Ca yield is confirmed, then the observations strongly support a variable IMF (at the upper end only) where more massive galaxies tend to form more of the most massive stars. In any case, the Ca trend does not particularly favor the scenario of timescale modulated Type II vs. Type Ia supernova enrichment effectiveness that has received most mention in the literature to date.

Major funding was provided by the National Science Foundation grant AST-0346347. The authors thank E. Toloba, P. Sánchez-Blázquez, and S. C. Trager for providing their spectral data.

REFERENCES

- Bender, R., Burstein, D., & Faber, S. M. 1993, *ApJ*, 411, 153
- Blakeslee, J. P., et al. 2009, *ApJ*, 694, 556
- Buzzoni, A. 1989, *ApJS*, 71, 817
- Cenarro, A. J., Gorgas, J., Vazdekis, A., Cardiel, N., & Peletier, R. F. 2003, *MNRAS*, 339, L12
- Cenarro, A. J., Sánchez-Blázquez, P., Cardiel, N., & Gorgas, J. 2004, *ApJ*, 614, L101
- Davies, R. L., Sadler, E. M., & Peletier, R. F. 1993, *MNRAS*, 262, 650
- Dotter, A., Chaboyer, B., Ferguson, J. W., Lee, H.-c., Worthey, G., Jevremović, D., & Baron, E. 2007, *ApJ*, 666, 403
- Faber, S. M., Worthey, G., & González, J. J. 1992, in *IAU Symp. 149, The Stellar Populations of Galaxies*, ed. B. Barbuy & A. Renzini (Dordrecht: Kluwer), 255
- Graves, G. J., Faber, S. M., Schiavon, R. P., & Yan, R. 2007, *ApJ*, 671, 243
- Grevesse, N., & Sauval, A. J. 1998, *Space Sci. Rev.*, 85, 161
- Henry, R. B. C., & Worthey, G. 1999, *PASP*, 111, 919
- Kobayashi, C., Umeda, H., Nomoto, K., Tomimaga, N., & Ohkubo, T. 2006, *ApJ* 653, 1145
- Kuntschner, H. 2000, *MNRAS*, 315, 184
- Kuntschner, H., et al. 2006, *MNRAS*, 369, 497
- Lee, H.-c. et al. 2009, *ApJ*, 694, 902
- Nomoto, K., et al. 2006, *Nucl. Phys. A*, 777, 424
- O’Connell, R. W. 1976, *ApJ*, 206, 370
- Peletier, R. F. 1989, PhD thesis, Univ. of Groningen
- Peterson, R. C. 1976, *ApJ*, 210, L123
- Poole, V., Worthey, G., Lee, H.-c., & Serven, J. 2010, *AJ*, 139, 809
- Press, W. H., Teukolsky, S. A., Vetterling, W. T., & Flannery, B. P. 1992, *Numerical Recipes in FORTRAN*, (2nd ed.: Cambridge: Cambridge University Press)
- Prochaska, L. C., Rose, J. A., & Schiavon, R. P. 2005, *AJ*, 130, 2666
- Rawle, T. D., Smith, R. J., & Lucey, J. R. 2010, *MNRAS*, 401, 852
- Saglia, R. P., Maraston, C., Thomas, D., Bender, R., & Colless, M. 2002, *ApJ*, 579, L13
- Salpeter, E. E. 1955, *ApJ*, 121, 161
- Sánchez-Blázquez, P., Gorgas, J., Cardiel, N., & González, J. J. 2006a, *A&A*, 457, 787
- Sánchez-Blázquez, P., et al. 2006b, *MNRAS*, 371, 703
- Schwarzschild, K., & Eberhard, G. 1913, *ApJ*, 38, 292
- Serven, J., Worthey, G., & Briley, M. M. 2005, *ApJ*, 627, 754
- Serven, J. 2010, PhD thesis, Washington State University
- Serven, J., Worthey, G., Toloba, E. 2010, & Sánchez-Blázquez, P. 2011, *AJ*, 141, 184
- Smith, R. J., Lucey, J. R., Hudson, M. J., & Bridges, T. J. 2009, *MNRAS*, 398, 119
- Spinrad, H., & Taylor, B. J. 1971, *ApJS*, 22, 445
- Thomas, D., Maraston, C., & Bender, R. 2003, *MNRAS*, 343, 279
- Timmes, F. X., Woosley, S. E., & Weaver, T. A. 1995, *ApJS*, 98, 617
- Trager, S. C., Faber, S. M., & Dressler, A. 2008, *MNRAS*, 386, 715
- Trager, S. C., Worthey, G., Faber, S. M., Burstein, D., & González, J. J. 1998, *ApJS*, 116, 1
- Trager, S. C., Worthey, G., Faber, S. M., & Dressler, A. 2005, *MNRAS*, 362, 2
- Valdes, F., Gupta, R., Rose, J. A., Singh, H. P., & Bell, D. J. 2004, *ApJS*, 152, 251

- van Dokkum, P. G., & Conroy, C. 2010, *Nature*, 468, 940
- Vazdekis, A., Peletier, R. F., Beckman, J. E., & Casuso, E. 1997, *ApJS*, 111, 203
- Wheeler, J. C., Sneden, C., & Truran, J. W., Jr. 1989, *ARA&A*, 27, 279
- Wilson, O. C. 1959, *ApJ*, 130, 499
- Wilson, O. C., & Vainu Bappu, M. K. 1957, *ApJ*, 125, 661
- Woosley, S. E., & Weaver, T. A. 1995, *ApJS*, 101, 181
- Worthey, G. 1994, *ApJS*, 95, 107
- Worthey, G. 1998, *PASP*, 110, 888
- Worthey, G., Dorman, B., & Jones, L. A. 1996, *AJ*, 112, 948
- Worthey, G., España, A., MacArthur, L. A., & Courteau, S. 2005, *ApJ*, 631, 820
- Worthey, G., Faber, S. M., & González, J. J. 1992, *ApJ*, 398, 69
- Worthey, G., Faber, S. M., González, J. J., & Burstein, D. 1994, *ApJS*, 94, 687
- Worthey, G., & Ottaviani, D. L. 1997, *ApJS*, 111, 377

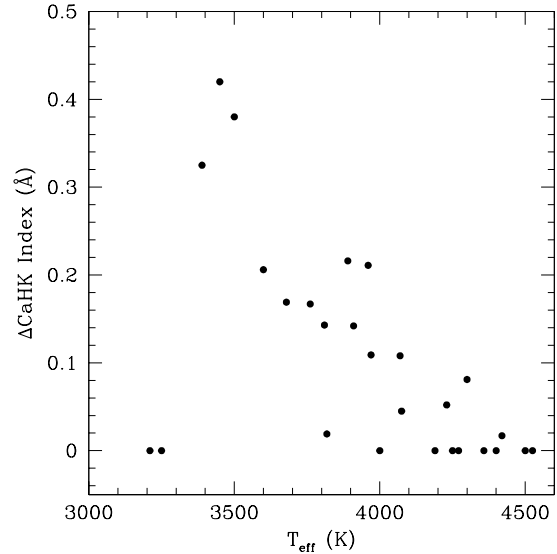


Fig. 6.— Trend of $\Delta\text{CaHK} = \text{CaHK}(\text{corrected}) - \text{CaHK}(\text{uncorrected})$ vs. T_{eff} for cool metal-rich giant stars selected from the Indo-US library of Valdes et al. (2004).

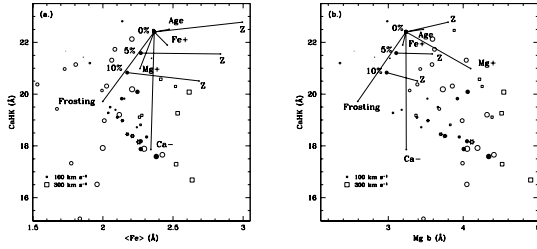


Fig. 7.— Modeling results in the CaHK vs. $\langle \text{Fe} \rangle$ (panel (a)) and Mg b (panel (b)) diagrams are shown. The shifted versions of the data are repeated from previous figures, sans error bars. Three heavy dots mark models of single-age populations, that age being 8 Gyr. The 0%, 5%, and 10% sequence refers to the fraction by mass of an additional metal-poor component of $[\text{M}/\text{H}] = -1.5$. The lighter dots indicate tweaks from that initial starting model. The ones marked “Z” refer to increasing lockstep heavy element abundance by 0.25 dex. In the case of the metallicity-composite models, only the metal-rich, dominant component changes its abundance. The other labels have the following meanings. “Age” means an age increase from 8 Gyr to 12 Gyr, “Frosting” is a 10% by mass addition of a 1 Gyr age, solar abundance component, “Ca−” is a drop of $[\text{Ca}/\text{R}]$ of -0.15 , “Fe+” is an increase of $[\text{Fe}/\text{R}]$ of $+0.05$, and “Mg+” is an increase of $[\text{Mg}/\text{R}]$ of $+0.2$.

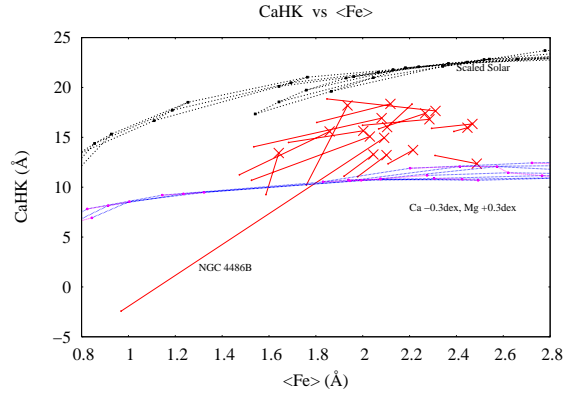


Fig. 8.— CaHK and $\langle \text{Fe} \rangle$ gradient trends. Using only the Servén (2010) data set, gradient trends within each galaxy are plotted with line segments connecting averages of the near-nuclear spectra with averages of the outer parts of the light along the slit. The model grids contain ages 1.5, 2, 3, 5, 8, 12, 17 Gyr populations and metallicities $[\text{M}/\text{H}] = -2, -1.5, -1.0, -0.5, -0.25, 0, 0.25$, and 0.5 , with no ages less than 8 Gyr plotted for metallicities less than -0.25 . The lower set of models is identical except that, at the spectral level, 0.3 dex more Mg and 0.3 less Ca is included. This alters Z in a slightly positive way, but leaves all heavy element ratios unaltered except those involving Mg or Ca.

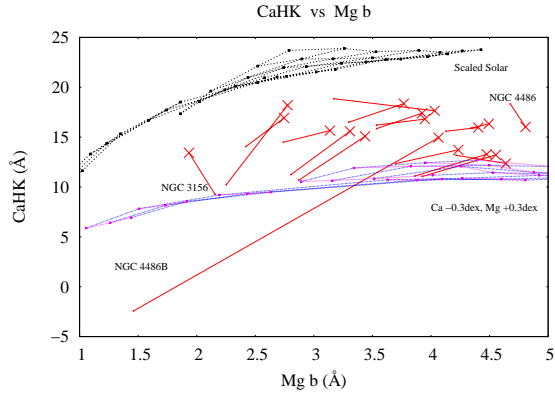


Fig. 9.— CaHK and Mg b gradient trends. Using only the Serven (2010) data set, gradient trends within each galaxy are plotted with line segments connecting averages of the near-nuclear spectra with averages of the last reliable outer measurement along the slit. Models are as in Fig. 8. NGC 3156 is dominated by a ~ 1 Gyr young stellar population and also appears to buck the gradient trend defined by the other galaxies somewhat.